APL Materials

Two-dimensional crystals of mesoporous silica SBA-15 nanosheets with perpendicular and open channels

Cite as: APL Mater. 2, 113303 (2014); https://doi.org/10.1063/1.4897203
Submitted: 28 July 2014 . Accepted: 22 August 2014 . Published Online: 10 October 2014

Yi-Qi Yeh, Chih-Yuan Tang, and Chung-Yuan Mou

AIP Publishing

Two-dimensional crystals of mesoporous silica SBA-15 nanosheets with perpendicular and open channels

Yi-Qi Yeh,[1] Chih-Yuan Tang,[2] and Chung-Yuan Mou[3,a]
[1]*National Synchrotron Radiation Research Center, Hsinchu 30077, Taiwan*
[2]*Instrumentation Center, National Taiwan University, Taipei 106, Taiwan*
[3]*Department of Chemistry, National Taiwan University, Taipei 10617, Taiwan*

(Received 28 July 2014; accepted 22 August 2014; published online 10 October 2014)

A preparation of mesoporous silica SBA-15 thin sheets with perpendicular nanochannels (SBA(⊥)) and open ends is reported here. At a synthesis condition of pH = 2 where the silica condensation is extremely slow, micron-sized single-crystal-like hexagonally faceted nanosheets (SBA(⊥)-pH2) with aspect ratio of 10–50 were formed. The nanosheets can attach to each other in sideway to extend the thin sheet. At pH = 5, multi-domain SBA(⊥)-pH5 nanosheets are formed, and stacking attachment of sheets is preferred. Vivid Moiré patterns are observed in large areas of stacked silica sheets, indicating excellent structure order. [http://dx.doi.org/10.1063/1.4897203]

Controlling morphology of ordered mesoporous materials (OMM) is important in many of its applications such as in nanofiltration[1] and catalyst support[2] which requires careful consideration in designing channel length and orientation. Among the OMM, extensive efforts have been devoted to synthesize SBA-15 of different morphologies,[3] such as spheres, fibers,[4] hexagon rods,[5] hexagonal platelets,[6,7] and supported film.[8] However, there have been few reports on free-standing nanosheet form with open perpendicularly oriented pore which would be very useful in many applications.[9,10] It is expected this kind of 2D porous materials would have excellent potential in catalyst supports (for its short pore length), nano-filtration (for easy stacking on large area grids) and mask for nano-electronics (for its sub 10 nm periodical perpendicular pores). Channel orientation of thin film of mesoporous silica on solid surface can be guided by external interactions such as nano-scale epitaxy,[11] strong magnetic field,[12] flow control[13] and surface micellar packing,[14] to more or less partial success. These "external" methods are not available to the free-standing thin nanosheet for guiding the formation of perpendicular pores. The material has to be self-assembled from a solution composition.

Although mesoporous silica SBA-15 of free standing platelet form has been reported before,[6,7,9,10] it is still very hard making free standing 2D crystal-like nanosheets of SBA-15 with (1) aspect ratio higher than 20 (lateral dimension/thickness) and (2) perpendicular channels with open pore entrance at both ends. The difficulty is due to fact that aggregations of rigid micellar rods favoring large lateral the dimension also tend to be very long. In simple words, cutting growth only along rod axis dimension is not "natural". The perpendicular direction has to be confined in synthesis. Previously,[10,15] we reported a synthesis of SBA-15 with the neutral triblock copolymer (P123) and a silica precursor confined between bilayers of a mixed cationic/anionic surfactant system (cetyltrimethylammonium bromide, CTAB and sodium dodecylsulfate, SDS) and obtained free-standing mesoporous silica nanosheet with vertical channels. The surface of (001) was stopped from growing by the passification of CTAB/SDS bilayer. However, the obtained nanosheets are not rigidly flat; there are undulations of the nanosheet. This indicates bending rigidity was somewhat low, unfavorable for growing into larger size. In this work, we would like to be able to control the bending rigidity of the nanosheet such that flat large-area 2D single crystal-like morphology can be

[a]E-mail: cymou@ntu.edu.tw

obtained. We will do this by varying the pH value of the synthesis condition such that silica condensation rate can be slowed down to the extent that high quality single crystal-like nanosheet can be obtained. The second goal of this work is to study interactions between the nanosheet along both in-plan direction and stacking direction. We would like to find out the condition for self-oriented attachment of the nanosheets.

The preparation of SBA(⊥) follows a modified method of that in our previous study.[15] In a typical surfactant mixture preparation, 0.75 g CTAB, 0.89 g SDS, and 0.7 g P123 were dissolved in 150 g H_2O under stirring at 45 °C to form a homogeneous solution. The dilute silicate solution was also prepared by mixing 2.75 g sodium silicate (27 wt. %) and 150 g 0.04 M $H_2SO_{4(aq)}$ solution. The pH values of surfactant and silicate solutions were adjusted to 5 before mixing. After vigorously stirring for 1 min, the resulting solutions were kept at static condition at 45 °C for 1 day. The as-synthesized SBA(⊥)-pH5 was obtained. In SBA(⊥)-pH2 preparation, the dilute silicate solution was prepared by mixing the same dosages of sodium silicate and $H_2SO_{4(aq)}$ solution, following by adjusting pH value to 4.3 for 3 min. Then, the pH values of surfactant and silicate solutions were adjusted to 2.0 before mixing. It turns out the 3 min equilibration step at pH = 4.3 is very crucial for making rigid single crystal nanosheet (to be discussed later). After vigorously stirring for 1 min, the resulting solutions were kept at static condition at 45 °C for 3 days. The as-synthesized samples were collected by filtration and hydrothermally treated in deionized water at 373 K for 24 h before calcination at 873 K for 6 h. The nitrogen adsorption isotherms and XRD patterns (Fig. S1)[26] are employed to give textural properties of SBA(⊥)-pH5 and SBA(⊥)-pH2 (after hydrothermal), including total Brunauer-Emmett-Teller (BET) surface area (694 and 626 m^2/g), microporous surface area (65 and 5 m^2/g), pore sizes (9.5 and 8.4 nm), pore volumes (1.214 and 0.820 cm^3/g), unit cell dimension (11.6 and 11.3 nm), and wall thickness (2.1 and 2.9 nm), respectively. (For structural properties, please see Table S1 in the supplementary material.[26])

Fig. 1 shows EM images of SBA(⊥) synthesized at pH 5 (SBA(⊥)-pH5) and SBA(⊥) synthesized at pH 2 (SBA(⊥)-pH2). The top row of Fig. 1 gives the results for SBA(⊥)-pH5. In Fig. 1(a_1), SEM image shows the single layer micron-sized sheet morphology of calcined SBA(⊥)-pH5. Ultrathin microtomed TEM images of as-synthesized SBA(⊥)-pH5 are given in Figs. 1(a_2) and 1(a_3). Fig. 1(a_2) reveals the silica sheets of homogeneous thickness between 60 and 100 nm and the

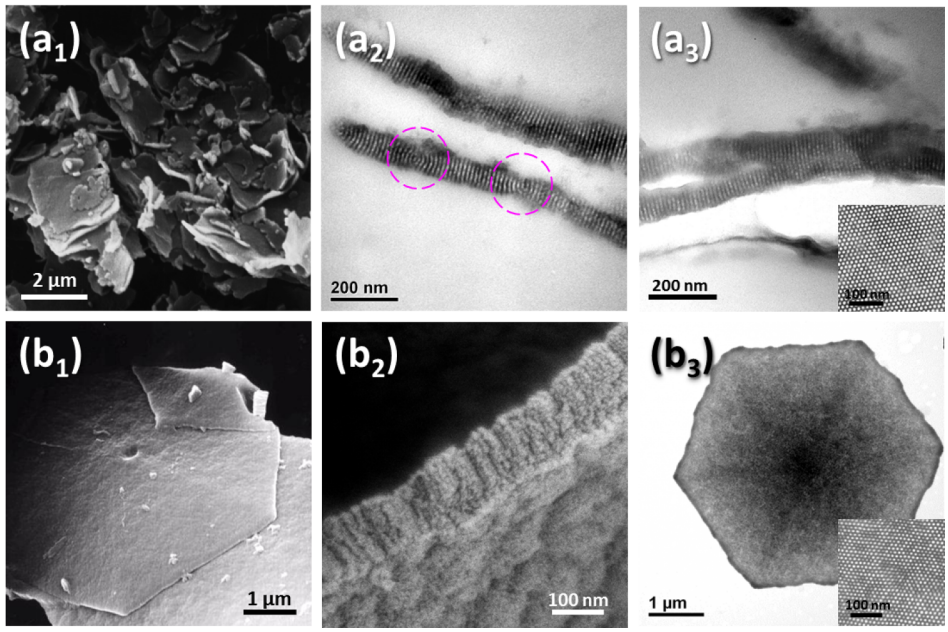

FIG. 1. (a_1) SEM images of calcined SBA(⊥)-pH5. Ultrathin microtomed TEM images of as-synthesized SBA(⊥)-pH5: (a_2) single-layer sheet and (a_3) two-layer stacking sheets. The attaching point between two domains is depicted by dashed circle. (b_1) SEM image and (b_2) HR-SEM (High-Resolution Scanning Electron Microscope) image of calcined SBA(⊥)-pH2. (b_3) TEM image of as-synthesized SBA(⊥)-pH2. The insets in (a_3) and (b_3) show the high-magnitude TEM images.

well-aligned perpendicular nanochannels. Previously, we have proposed the formation of such kind of thin nanosheet is due to the confinement of mixed cationic/anionic surfactant system CTAB/SDS. Such confinement effect apparently decreased the surface free energy of (001) faces of SBA(⊥) and led to the formation of SBA(⊥) thin silica sheet with high height to width ratio. The aspect ratios of the nanosheet were in the much higher range of 10–50 in comparison with previously reported platelet SBA-15 of A(001)/A(100) in the range of 1.25-2.75.[7] The nanochannels are open at both ends while at the edges they show bending behavior to give the rounded edges. In some places in the middle (depicted by red circles in Fig. 1(a_2)), the nanochannel ordering is abruptly changed and appears like in the edge region. It suggests side-way attachment of two separate lattice domains. Fig. 1(a_3) shows that two separate layers of SBA(⊥)-pH5 merge into a thicker one, in which the nanochannels continue from the top to the bottom surface. The inset in Fig. 1(a_3) shows the well-ordered 2D hexagonally arrayed mesopores. These results suggest that the single-layer nanosheet SBA(⊥)-pH5 is composed of several domains with well-aligned perpendicular nanochannels.

The bottom row of Fig. 1 gives the results for SBA-15 synthesized at pH = 2, e.g., SBA(⊥)-pH2. In Fig. 1(b_1), the SEM image shows a single-layered, flat and rigid hexagonal sheet morphology of calcined SBA(⊥)-pH2. In Fig. 1(b_2), the cross-section SEM image of calcined SBA(⊥)-pH2 shows that the single-layer sheet with homogeneous thickness of ~120 nm and aligned perpendicular nanochannels. In Fig. 1(b_3), as-synthesized SBA(⊥)-pH2 displays sheet morphology of several micrometer-sized, faceted hexagons with well-ordered 2D hexagonally arrayed mesopores (inset). N_2 sorption isotherms and XRD patterns (Fig. S1) confirm uniform pore size and well-ordered 2D hexagonal mesostructure of SBA(⊥)-pH5 and SBA(⊥)-pH2.

Fig. 2 gives the TEM image of as-synthesized SBA(⊥)-pH5. It shows well-ordered arrangements of 2D hexagonal pores of the perpendicular channels, with many domains. The orientation of each domain is depicted by an arrow. Each domain exhibits the same hexagonal symmetry while they rotated by certain angles with respect to each other. The domain boundaries between neighboring domains are well-defined in the form of narrow border (shown by dashed line). This is consistent with the boundary region of cross-sectional view shown in Fig. 1(a_2) One can observe single-layer silica sheet of multi-domain with 2D hexagonally arrayed nanochannels in SBA(⊥)-pH5. It suggests that two hexagonal lattice domains of SBA(⊥)-pH5 thin sheets can be attached side-way during formation.

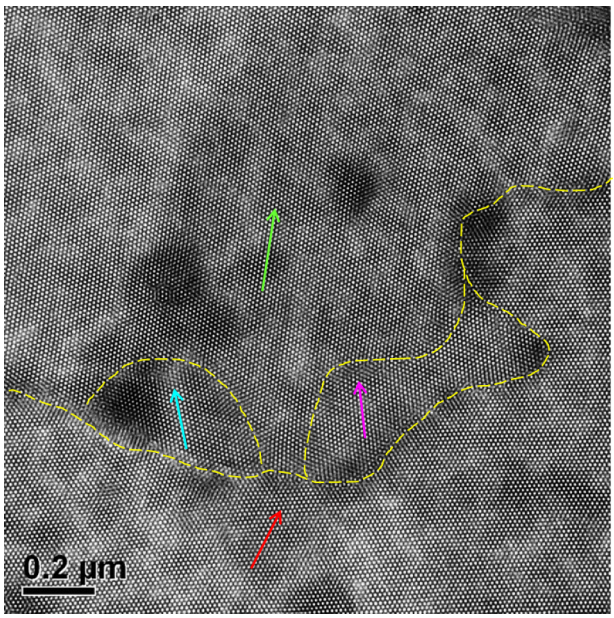

FIG. 2. TEM images of as-synthesized SBA(⊥)-pH5. The orientation of each domain is depicted by arrow. The domain boundary is indexed by dashed line.

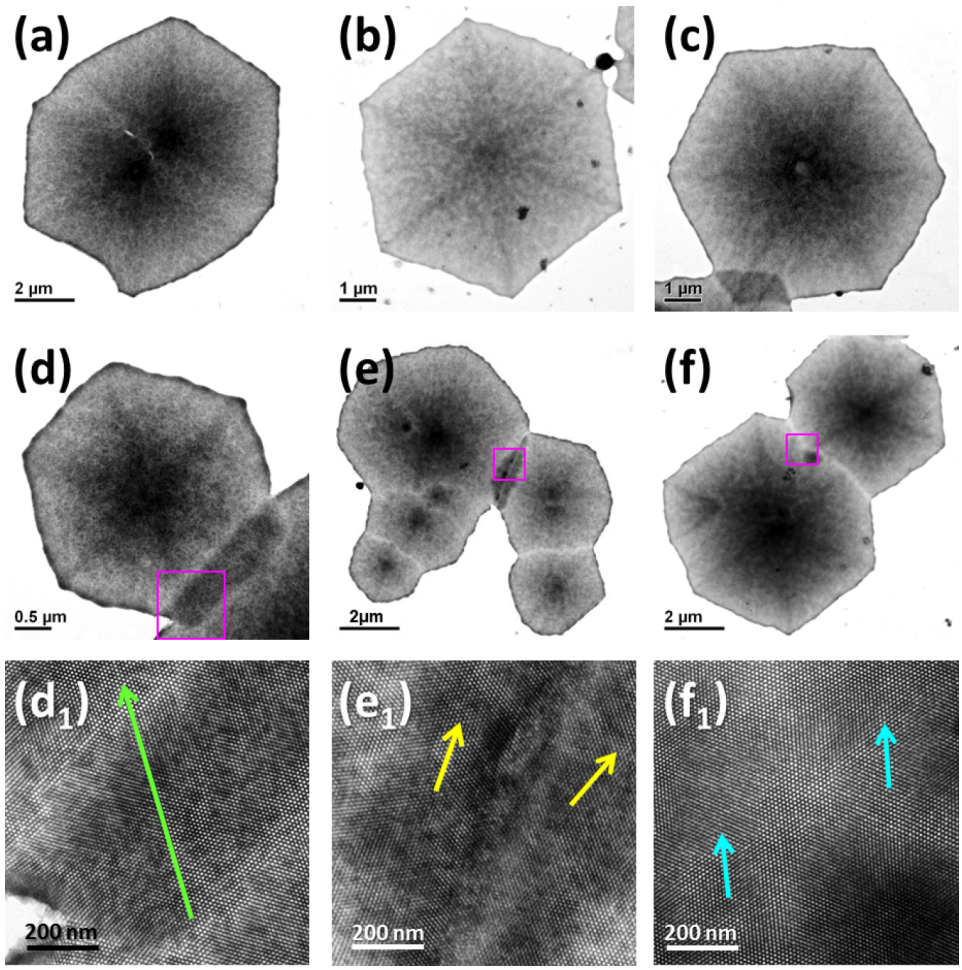

FIG. 3. TEM images for as-synthesized SBA(⊥)-pH2. (a)-(c) Hexagonal silica sheets, (d)-(f) polygonal silica sheets. (d_1)-(f_1) Enlarged images of the boxed areas depicted in (d)-(f). The orientation of each domain is depicted by an arrow.

Fig. 3 shows the TEM results of SBA(⊥)-pH2. The top row (Figs. (a)-(c)) shows the hexagon-faceted sheet morphology of 6-9 μm in size. The regular hexagons exhibit single-crystal character with 2D hexagonally arrayed mesopores. Along the six-fold symmetry axis, the "ridges" seem to be a little thicker. The hexagons are large and very thin with aspect ratios A(001)/A(100) between 10 and 50 which is much higher than for the disk morphology reported for SBA-15.[6,7] Figures 3(d)-3(f) displays the connected hexagonal silica sheets when they meet each other. They attach to each other sideway. Figures 3(d_1)-3(f_1) show the enlarged images of the boxed areas in Figs. 3(d)-3(f). The orientation of each domain is depicted by an arrow. In Fig. 3(d_1), one can observe the same orientation across the two separate sheets. It suggests single-domain character in the two connecting hexagonal sheets. Fig. 3(e_1) shows the associated region of two polygonal silica sheets in the boxed area of Fig. 3(e). One can observe the domain boundary appeared in the overlapping region between two individual single-domain lattices. The domain boundary might derive from stress relaxation in the solid phase inherited from the attachment.[16] In Fig. 3(f_1), the edge-attaching region between two separate hexagonal sheets displays continuously well-ordered 2D hexagonally arrayed mesopores. However, there is a small mis-orientation (~2°) of the two neighboring single-domain sheets, called dislocation in crystallography, possibly due to strain relaxation between two lattice domains. For the case of pH = 2 synthesis, the attaching of two neighboring lattice domains could be epitaxial forming perfectly single-domain or the edge-attaching region of two neighboring lattice domains forming dislocation. It seems that the two neighboring domains with 2D hexagonal arrayed nanochannels of SBA(⊥)-pH2 prefer attaching along (001) face in attachment.

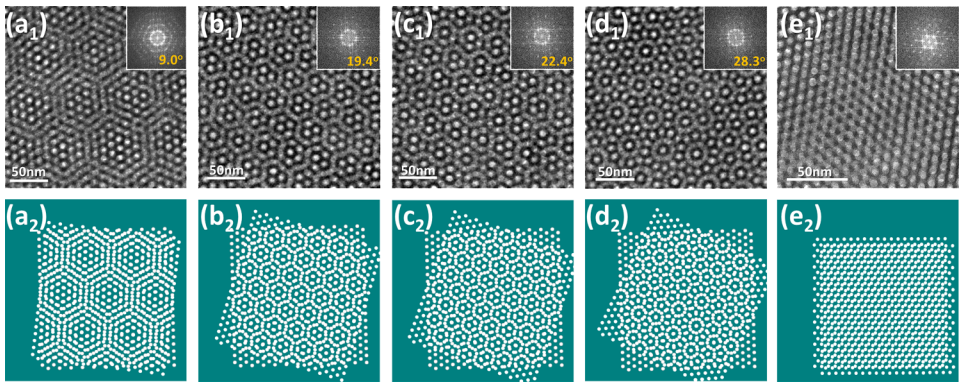

FIG. 4. (a_1)-(e_1) HR-TEM images and the corresponding of FFT spectrum (inset) of Moiré patterns arising from two-layer stacking sheets of as-synthesized SBA(⊥)-pH5. The corresponding structural models of two-layer hexagonal lattices stacking are shown in (a_2)-(e_2). The rotation angles between top and bottom hexagonal lattices are (a_2)9°, (b_2) 19.4°, (c_2) 22.4°, and (d_2) 28.3°. (e_2) The translation Moiré pattern with a spacing offset.

For the pH = 5 synthesis, the nanosheet gave irregular domain boundary for in-plan relative orientations. However, overall we also see a lot of vertical stacking of the nanosheets. The relative orientations of the stacking can be evaluated through the observation of Moiré pattern of the hexagonal lattice. In Fig. 4, detailed TEM observation showed five examples of pseudo-periodic patterns found in SBA(⊥)-pH5. According to previous studies,[17–19] such periodic patterns are due to rotation and translation Moiré patterns in the stacking of two identical periodic patterns. To understand the pseudo-periodic patterns, we study the 2-D fast Fourier transform (FT) spectrum of these periodic structures and propose a structural model of 2D hexagonally arrayed spots, maintaining the same ratio as the original structure feature of SBA(⊥)-pH5. Fig. 4(a_1) reveals a hexagonal feature and the corresponding FT pattern in inset. Its FT pattern gives 12 diffraction spots in main peaks with basic frequency, which can be grouped into two sets. Each set contains the same spacing and 6 spots that are related with each other by a 6-fold rotational symmetry. This reflected the six-fold rotational symmetry of SBA(⊥) and the two sets were relatively rotated by 9° as marked by two arrows. Thus, we drew a structural model of two hexagonal lattices, rotated by 9° to each other from the intersecting point in Fig. 4(a_2). The structural model is consistent with the observed image in Fig. 4(a_1). This suggested that there exist two separate layers of hexagonal mesostructured sheets which rotated by an angle 9° along [001] direction. Fig. 4(a_1) revealed a hexagonal superstructure with periodicity about 75 nm. The theoretical value, according to the Rayleigh relation for the feature size of rotation Moiré fringes $D = d/[2\sin(\alpha/2)]$,[17] is calculated as 71 nm—close to the measured value.

Figs. 4(b_1)-4(d_1) shows the rotation Moiré patterns with the relative rotation angles 19.4°, 22.4°, and 28.3°, as revealed by the corresponding FFT spectrum. Also, the structural models (Figs. 4(b_2)-4(d_2)) were in consistent with the observed images (Figs. 4(b_1)-4(d_1)). Besides, we have observed the translation Moiré pattern in Fig. 4(e_1). Its FT pattern has 6 diffraction spots in main peaks by a 6-fold rotational symmetry. This suggested that the overlapping layers have the same orientation but displaced by a translation shift. In Fig. 4(e_2), the structural model of two hexagonal latticed displaced to each other by a translational spacing offset is similar to the observed image (shown in Fig. 4(e_1)). The rotation Moiré patterns are produced by the 6-fold symmetry of SBA(⊥)-pH5 and the patterns with relative angles ranging within 9°-30° have been observed. Rotation Moiré patterns from offsets smaller than 9° can be hardly observed because of the limited domain size of SBA(⊥)-pH5 (shown in Fig. 2). Thus we propose that the observed Moiré patterns are derived from random stacking of two-layer SBA(⊥) nanosheets. Fig. 5 displays 3D electron microscopic tomography observation of SBA(⊥)-pH5. The slice images in 2D plane showed the basic morphology after reconstruction. The central image (Fig. 5(a_1)), revealing super-periodic pattern, was observed directly in the xy plane. The left-side image (Fig. 5(a_2)) shows a slice image through reconstruction in the yz plane along the green line.

The bottom image (Fig. 5(a_3)) is a slice image through reconstruction in the xz plane along the red line. The yz slice displayed the two silica sheets with homogeneous sheet thickness,

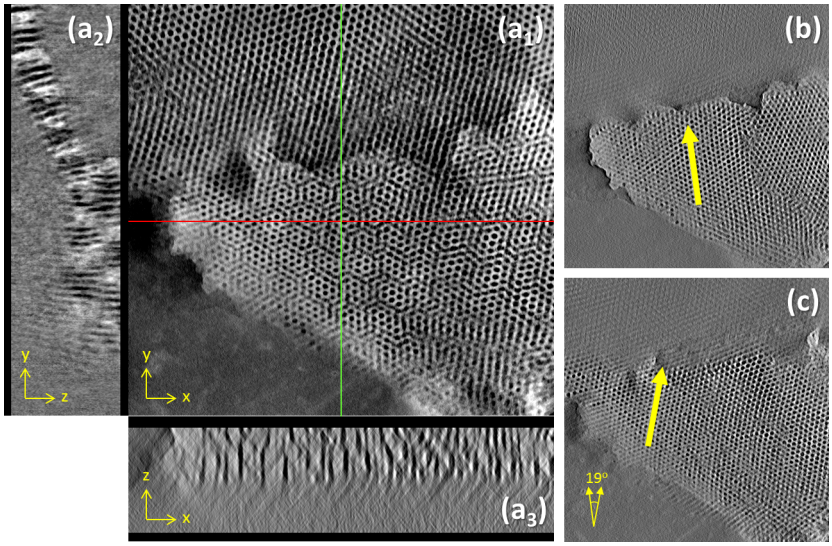

FIG. 5. 3D electron tomography results of hydrothermally treated and calcined SBA(⊥)-pH5 in (a_1) XY-plane, (a_2) YZ-plane along vertical (green) line, and (a_3) XZ-plane along horizontal (red) line. The basic morphologies of as-synthesized SBA(⊥) were reconstructed when focusing on upper layer (b) and focusing on the bottom layer (c). The mis-orientation angle is 19° between the two layers.

well-aligned perpendicular nanochannels, and the same lattice spacing. These slice results show that the two silica sheets stacked along the sheet plane into a thicker one and revealed continuous straight nanochannels from the top to the bottom surface. The basic morphology of two separate sheets were reconstructed when focusing on upper layer (Fig. 5(b)) and focusing on the bottom layer (Fig. 5(c)). The arrows depicted in Figs. 5(b) and 5(c) exhibited the orientation of the reconstructed silica sheet. The relative angle between them was measured about 19°. The 3D tomography results strengthen further the proposed superimposition of two-layer SBA(⊥)-pH5 silica sheets.

One should note here that Moiré patterns have been observed in mesoporous silica by TEM before.[16,21] But they were formed from grain boundary dislocations in a monolith structure. The angle of rotation was thus limited, and the domain size is rather small. In this work, we report the emergence of micron-sized single-domain hexagonal SBA(⊥) sheets and Moiré pattern from two stacked SBA(⊥) sheets. Moiré patterns have been observed in other overlapping periodical structures, such as self-assembly of multilayer hexagonal DNA arrays,[18,19] and STM observation of deposited metal-on-metal surface,[20] bilayer graphenes,[21] or porous alumina.[22] Creating lithographic Moiré patterns would be highly interesting for nanoelectronic applications. Recently, there is a rising interest in using block copolymer as nanolithography mask because of the parallel nature of the sub-20 nm patterning process.[17,23] However, it is not robust under long time electron irradiation. The nanosheet of SBA(⊥) with 2D hexagonal arrangement of uniform perpendicular silica pores may prepare for a development in nanolithography.

A potential use of SBA(⊥) may be in nanofiltration membrane. Since it possesses short nanochannels with open-ended pores, the two (often conflicting) criteria of good size selection and high permeability could be attained at the same time. One may deposit the mesoporous silica nanosheets directly on macroporous anodized aluminum oxide (AAO) supports for fabricating mesoporous silica membranes.[24] With pore size in the 5 to 10 nm range, it may be developed as a nanofilter for the separation of protein or polymers. An indirect use of SBA(⊥) is in electrocatalysis; previously Lin *et al.* have used the SBA-15(⊥) as hard template to make mesoporous carbon with perpendicular channels. With deposited PtRu catalyst, the materials were deposited on anodes in direct fuel methanol cell. The stacking of the mesoporous carbon nanosheets on the electrode was responsible for the excellent activity.[25]

Finally, we would like to come back to comment on the main difference in the formation of hexagons of SBA-15 nanosheets at pH = 2. The rigid hexagons are not only good-looking but also

useful in new applications as they are easy to stack and attach. Two key concepts in our synthesis design are membrane confinements and strong segregation of P123 and silicates. The bi-layer membranes of SDS/CTAB confine the synthesis of SBA-15 to a thin sheet and make perpendicular orientation of pores possible.[10] The strong segregation of P123 and silicates make good and rigid mesostructure possible. Previously,[15] we did show that decreasing pH value of synthesis would lead to stronger segregation of silicates and P123, and thus a synthesis at pH = 2 presumably would lead to the most rigid (thus flat and no undulating) nanosheet. If we used our previous procedure in Ref. 15 (e.g., direct adjusting pH to 2), however, we got mixtures of particles and disk with channels parallel to the disk surface (as shown in Fig. S3).[26] The stronger segregation at pH = 2 also led to parallel orientation of nanochannels. So there is a dilemma in here which we did not know how to solve in 2011. Now, we find the adjustment of pH = 4.3 at intermediate before setting to pH = 2 is very important. It represents that less strong segregation (at pH = 4.3) of Poly(propyl oxide) (PPO) and Poly(ethylene oxide) (PEO)/silicate segments and decreasing strength of the wall-segment interaction; hence, walls repel less to PEO/silicates and it gives rise to vertical nanochannel morphology. This allows the formation of nanosheet with perpendicular channels first at pH = 4.3 then the stronger segregation at pH = 2 allows the slow formation of rigid hexagons.

This research was supported by the National Science Council of Taiwan (NSC 98-2120-M-002-00298-2120-M-002-002).

[1] Z. K. Sun, Y. H. Deng, J. Wei, D. Gu, B. Tu, and D. Y. Zhao, Chem. Mater **23**(8), 2176 (2011); S. El-Safty, A. Shahat, M. R. Awual, and M. Mekawy, J. Mater. Chem. **21**(15), 5593 (2011).
[2] C. He, X. Y. Zhang, S. K. Gao, J. S. Chen, and Z. P. Hao, J. Ind. Eng. Chem. **18**(5), 1598 (2012); D. S. Yang, D. Bhattacharjya, S. Inamdar, J. Park, and J. S. Yu, J. Am. Chem. Soc. **134**(39), 16127 (2012); A. Szegedi, M. Popova, K. Lazar, S. Klebert, and E. Drotar, Microporous Mesoporous Mater. **177**, 97 (2013); G. Prieto, A. Martinez, R. Murciano, and M. A. Arribas, Appl. Catal. A **367**(1–2), 146 (2009).
[3] H. I. Lee, J. H. Kim, G. D. Stucky, Y. F. Shi, C. Pak, and J. M. Kim, J. Mater. Chem. **20**(39), 8483 (2010).
[4] K. Kosuge, T. Sato, N. Kikukawa, and M. Takemori, Chem. Mater. **16**(5), 899 (2004); M. C. Chao, C. H. Chang, H. P. Lin, C. Y. Tang, and C. Y. Lin, J. Mater. Sci. **44**(24), 6453 (2009).
[5] A. Sayari, B. H. Han, and Y. Yang, J. Am. Chem. Soc. **126**(44), 14348 (2004).
[6] Sujandi, S. E. Park, D. S. Han, S. C. Han, M. J. Jin, and T. Ohsuna, Chem. Commun. **2006**(39), 4131 ; X. G. Cui, S. W. Moon, and W. C. Zin, Mater. Lett. **60**(29–30), 3857 (2006); S. Y. Chen, C. Y. Tang, W. T. Chuang, J. J. Lee, Y. L. Tsai, J. C. C. Chan, C. Y. Lin, Y. C. Liu, and S. F. Cheng, Chem. Mater. **20**(12), 3906 (2008).
[7] P. Linton, J. C. Hernandez-Garrido, P. A. Midgley, H. Wennerstrom, and V. Alfredsson, Phys. Chem. Chem. Phys. **11**(46), 10973 (2009).
[8] K. C.-W. Wu, X. F. Jiang, and Y. Yamauchi, J. Mater. Chem. **21**, 8934 (2011); Y. Yamauchi, T. Nagaura, and S. Inoue, Chem-Asian J. **4**(7), 1059 (2009).
[9] E. M. Johansson, J. M. Cordoba, and M. Oden, Microporous Mesoporous Mater. **133**(1–3), 66 (2010).
[10] B. C. Chen, H. P. Lin, M. C. Chao, C. Y. Mou, and C. Y. Tang, Adv. Mater. **16**(18), 1657 (2004).
[11] E. K. Richman, T. Brezesinski, and S. H. Tolbert, Nat. Mater. **7**(9), 712 (2008).
[12] Y. Yamauchi, M. Sawada, T. Noma, H. Ito, S. Furumi, Y. Sakka, and K. Kuroda, J. Mater. Chem. **15**(11), 1137 (2005).
[13] B. Su, X. M. Lu, and Q. H. Lu, J. Am. Chem. Soc. **130**(44), 14356 (2008).
[14] Z. G. Teng, G. F. Zheng, Y. Q. Dou, W. Li, C. Y. Mou, X. H. Zhang, A. M. Asiri, and D. Y. Zhao, Angew. Chem., Int. Ed. **51**(9), 2173 (2012).
[15] Y. Q. Yeh, H. P. Lin, C. Y. Tang, and C. Y. Mou, J. Colloid Interface Sci. **362**(2), 354 (2011).
[16] R. H. Wang, Q. Chen, F. R. Chen, J. J. Kai, and L. M. Peng, Chem. Phys. Lett. **411**(4–6), 463 (2005); F. F. Xu, F. M. Cui, M. L. Ruan, L. L. Zhang, and J. L. Shi, Langmuir **26**(10), 7535 (2010).
[17] V. Luchnikov, A. Kondyurin, P. Formanek, H. Lichte, and M. Stamm, Nano Lett. **7**(12), 3628 (2007).
[18] Y. He, S. H. Ko, Y. Tian, A. E. Ribbe, and C. D. Mao, Small **4**(9), 1329 (2008); A. Y. Koyfman, S. N. Magonov, and N. O. Reich, Langmuir **25**(2), 1091 (2009).
[19] A. Singh, C. Dickinson, and K. M. Ryan, ACS Nano **6**(4), 3339 (2012).
[20] J. Weissenrieder, A. Gothelid, M. Mansson, H. von Schenck, O. Tjernberg, and U. O. Karlsson, Surf. Sci. **527**(1–3), 163 (2003).
[21] E. Sutter, D. P. Acharya, J. T. Sadowski, and P. Sutter, Appl. Phys. Lett. **94**(13), 133101 (2009).
[22] B. Chen and K. Lu, Langmuir **27**(7), 4117 (2011); J. S. Choi, R. B. Wehrspohn, and U. Gosele, Adv. Mater. **15**(18), 1531 (2003).
[23] C. J. Hawker and T. P. Russell, MRS Bull. **30**(12), 952 (2005); J. Y. Cheng, D. P. Sanders, H. D. Truong, S. Harrer, A. Friz, S. Holmes, M. Colburn, and W. D. Hinsberg, Acs Nano **4**(8), 4815 (2010).
[24] V. Boffa, J. E. ten Elshof, and D. H. A. Blank, Microporous Mesoporous Mater. **100**, 173 (2007).
[25] M. L. Lin, C. C. Huang, M. Y. Lo, and C. Y. Mou, J. Phys. Chem. C **112**(3), 867 (2008).
[26] See supplementary material at http://dx.doi.org/10.1063/1.4897203 for the experimental details and additional data, including the nitrogen adsorption isotherm and XRD patterns, SEM image of a hexagon 2D crystal of SBA(⊥)-pH2, SEM image and ultra-thin microtomed TEM image of mesoporous silica synthesized at pH2 and a table showing the textural properties of SBA(⊥)-pH5 and SBA(⊥)-pH2.